



Chromosome 10q26–driven age-related macular degeneration is associated with reduced levels of *HTRA1* in human retinal pigment epithelium

Brandi L. Williams^{a,1}, Nathan A. Seager^a, Jamie D. Gardiner^a, Chris M. Pappas^a, Monica C. Cronin^{a,2}, Cristina Amat di San Filippo^{a,3}, Robert A. Anstadt^a, Jin Liu^a, Marc A. Toso^a, Lisa Nichols^a, Timothy J. Parnell^b, Jacqueline R. Eve^{a,4}, Paul L. Bartel^{a,5}, Moussa A. Zouache^a, Burt T. Richards^a, and Gregory S. Hageman^{a,1}

^aSteele Center for Translational Medicine, John A. Moran Eye Center, University of Utah, Salt Lake City, UT 84132; and ^bBioinformatics Analysis, Huntsman Cancer Institute, University of Utah, Salt Lake City, UT 84132

Edited by Rando Allikmets, Columbia University Irving Medical Center, New York, NY, and accepted by Editorial Board Member Jeremy Nathans June 7, 2021 (received for review February 23, 2021)

Genome-wide association studies have identified the chromosome 10q26 (Chr10) locus, which contains the age-related maculopathy susceptibility 2 (*ARMS2*) and high temperature requirement A serine peptidase 1 (*HTRA1*) genes, as the strongest genetic risk factor for age-related macular degeneration (AMD) [L.G. Fritsche et al., *Annu. Rev. Genomics Hum. Genet.* 15, 151–171, (2014)]. To date, it has been difficult to assign causality to any specific single nucleotide polymorphism (SNP), haplotype, or gene within this region because of high linkage disequilibrium among the disease-associated variants [J. Jakobsdottir et al. *Am. J. Hum. Genet.* 77, 389–407 (2005); A. Rivera et al. *Hum. Mol. Genet.* 14, 3227–3236 (2005)]. Here, we show that *HTRA1* messenger RNA (mRNA) is reduced in retinal pigment epithelium (RPE) but not in neural retina or choroid tissues derived from human donors with homozygous risk at the 10q26 locus. This tissue-specific decrease is mediated by the presence of a noncoding, cis-regulatory element overlapping the *ARMS2* intron, which contains a potential Lhx2 transcription factor binding site that is disrupted by risk variant rs36212733. HtrA1 protein increases with age in the RPE–Bruch’s membrane (BM) interface in Chr10 nonrisk donors but fails to increase in donors with homozygous risk at the 10q26 locus. We propose that HtrA1, an extracellular chaperone and serine protease, functions to maintain the optimal integrity of the RPE–BM interface during the aging process and that reduced expression of *HTRA1* mRNA and protein in Chr10 risk donors impairs this protective function, leading to increased risk of AMD pathogenesis. HtrA1 augmentation, not inhibition, in high-risk patients should be considered as a potential therapy for AMD.

age-related macular degeneration | retinal pigment epithelium | Bruch’s membrane | *HTRA1* | cis-regulatory element

Age-related macular degeneration (AMD) affects nearly 200 million people worldwide with ~10 million patients suffering from late-stage disease characterized by severe vision impairment (1). AMD pathology typically initiates at the interface between the retinal pigment epithelium (RPE) and Bruch’s membrane (BM), which consists of an elastin layer confined between inner and outer collagenous layers. Collectively, the specialized RPE–BM structure forms a key component of the outer blood–retinal barrier and separates the neural retina from the choriocapillaris, the dense microvascular bed of the choroid (2). Hallmark phenotypes associated with AMD include the appearance of pathologic basal laminar deposits and/or soft drusen-like material beneath the RPE. Basal laminar deposits lie between the plasma membrane and basal lamina of the RPE and are thought to be comprised of polymerized long-spacing collagen and other extracellular matrix (ECM) proteins. Drusen generally form between the basal lamina and inner collagenous layer of BM and are composed of both lipids and proteins, including various complement pathway–associated proteins (3).

Over 34 genomic loci have been associated with elevated risk of AMD at a genome-wide significance level (4). While most of

these loci have minor impacts on the incidence of AMD (4, 5), genetic variants within the 10q26 region of chromosome 10 (Chr10) and the 1q32 region of chromosome 1 (Chr1) together account for more than 50% of AMD risk (6, 7). The 1q32 region contains the complement factor H (*CFH*) and complement factor H–related (*CFHR*) genes 1 to 5, while the 10q26 region contains the tightly linked age-related maculopathy susceptibility 2 (*ARMS2*) and high temperature requirement A serine peptidase 1 (*HTRA1*) genes. There are numerous coding and noncoding single nucleotide

Significance

The chromosome 10q26 locus is the genetic region most strongly associated with elevated risk of age-related macular degeneration (AMD), but the underlying genetic defects initiating disease are unresolved. Using human-derived eye tissues, we demonstrate that mRNA encoding the serine protease, *HTRA1*, is reduced in the retinal pigment epithelium (RPE) of donors with risk-associated variants that disrupt a cis-regulatory element within the 10q26 locus. Consequentially, there is diminished HtrA1 protein within the RPE–Bruch’s membrane interface, the primary site of AMD initiation, with age. This indicates that HtrA1 functions to maintain the integrity of this interface during the aging process and that HtrA1 levels are impaired by chromosome 10q26 risk-associated variants. HtrA1 augmentation may be a viable therapeutic option for AMD.

Author contributions: B.L.W., P.L.B., B.T.R., and G.S.H. designed research; N.A.S., J.D.G., C.M.P., M.C.C., C.A.d.S.F., R.A.A., J.L., M.A.T., and J.R.E. performed research; L.N., J.R.E., and M.A.Z. contributed new reagents/analytic tools; B.L.W., T.J.P., and M.A.Z. analyzed data; B.L.W. wrote the paper; L.N. coordinated donor eye collection and processing; and G.S.H. provided donor eye tissue, graded AMD status, critically reviewed work, and provided all funding.

Competing interest statement: G.S.H. is a shareholder, consultant, and cofounder of Voyant Biotherapeutics, LLC. G.S.H., C.M.P., B.T.R., and B.L.W. are inventors on patents and patent applications owned by the University of Utah.

This article is a PNAS Direct Submission. R.A. is a guest editor invited by the Editorial Board.

This open access article is distributed under [Creative Commons Attribution-NonCommercial-NoDerivatives License 4.0 \(CC BY-NC-ND\)](https://creativecommons.org/licenses/by-nc-nd/4.0/).

¹To whom correspondence may be addressed. Email: brandi.williams@hsc.utah.edu or gregory.hageman@hsc.utah.edu.

²Present address: Molecular Systems, Biochemistry R&D, BioFire Diagnostics, Salt Lake City, UT 84112.

³Present address: Infectious Diseases, Utah Public Health Laboratory, Taylorsville, UT 84129.

⁴Present address: Department of Pulmonology, Intermountain Healthcare, Murray, UT 84107.

⁵Present address: PharmaDX, ARUP Laboratories, Salt Lake City, UT 84112.

This article contains supporting information online at <https://www.pnas.org/lookup/suppl/doi:10.1073/pnas.2103617118/-DCSupplemental>.

Published July 22, 2021.

polymorphisms (SNPs) within the 10q26 region, as well as an insertion–deletion in the *ARMS2* 3' untranslated region (UTR). Efforts to determine which gene(s) or variant(s) within the chromosome 10 locus are causative for AMD have been hampered by the high linkage disequilibrium within this region (6, 8). A recent case-control study of individuals with rare recombinant haplotypes has narrowed the AMD-associated region to a block overlapping

ARMS2 exon 1 and intron 1 (9). Detectable expression and localization of *ARMS2* protein in human tissue and cells remains elusive, and the use of poorly characterized antibodies has resulted in conflicting reports (10–13). In contrast, HtrA1 protein is expressed in many tissues and functions as both a secreted serine protease and an extracellular chaperone (14). It forms multimeric trimers and hexamers and is activated by an allosteric mechanism

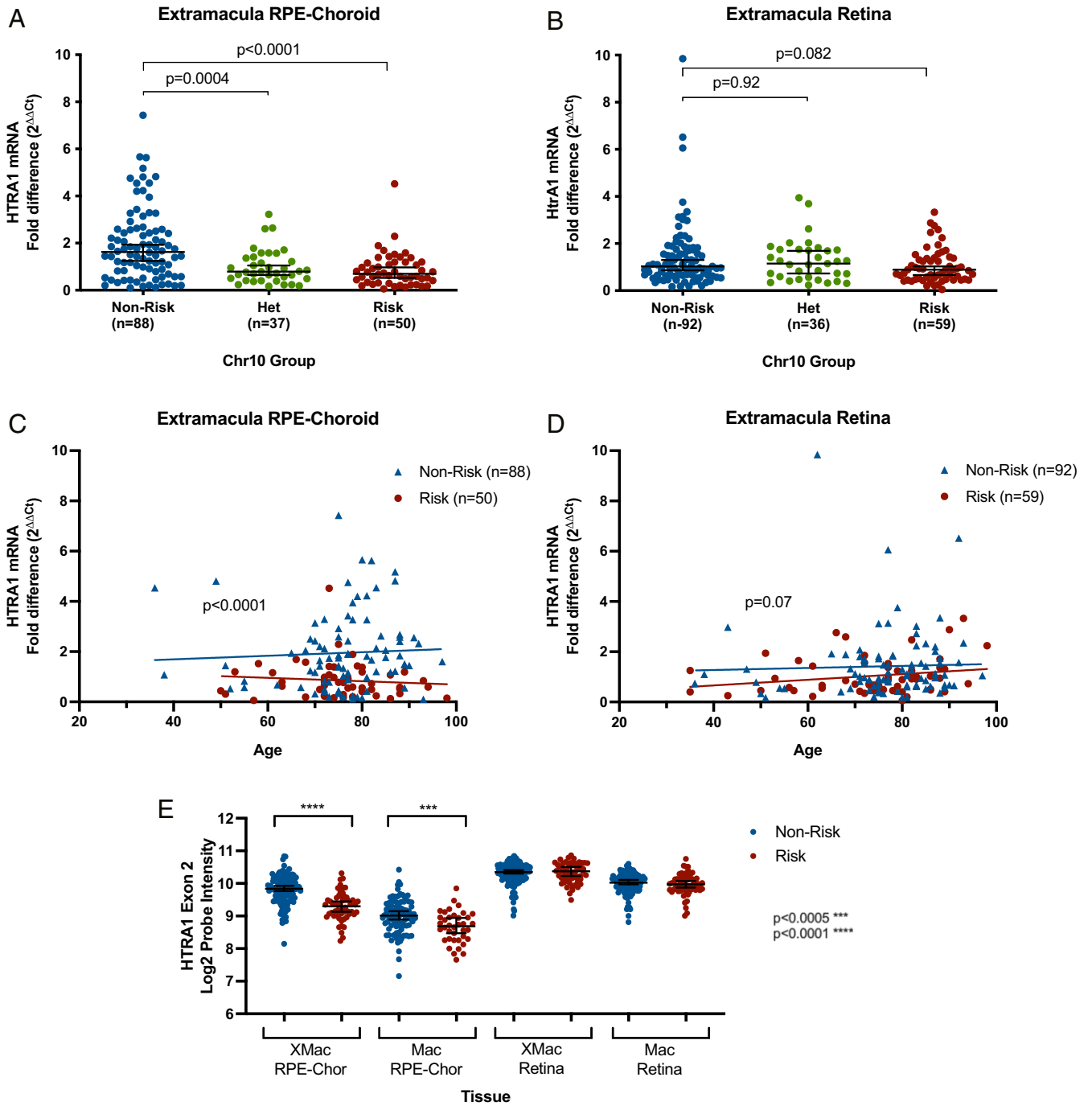


Fig. 1. Analyses of *HTRA1* mRNA levels in ocular tissues from human donors. (A and B) qRT-PCR analysis of *HTRA1* mRNA levels in extramacular RPE-choroid (A) or retina (B), comparing Chr10 genotype groups. Median values with 95% CI are shown. Mann–Whitney *U* test analysis was used to determine significance. (C and D) qRT-PCR analysis of *HTRA1* mRNA levels in extramacular RPE-choroid (C) or retina tissues (D), based on donor age. Tissue is from Chr10 homozygous nonrisk and risk groups. Linear regression analyses indicate the intercept of the two lines differ significantly between nonrisk and risk donors in RPE-choroid tissue ($P < 0.0001$) but not retina ($P = 0.07$). (E) Microarray analysis of *HTRA1* mRNA levels in extramacular (XMac) and macular (Mac) RPE-choroid and retina tissues using a probe targeting exon 2 of *HTRA1*. Donor tissue samples are from Chr10 homozygous nonrisk and homozygous risk genotype groups. Mann–Whitney *U* test analysis was used to determine significance. *** $P < 0.0005$, **** $P \leq 0.0001$.

to cleave a variety of ECM proteins, proteoglycans, and growth factors (15, 16).

The role of HtrA1 in ocular tissues is unclear, but insights can be derived from its functions in other diseases and from mouse models. Mutations in *HTRA1* that impair its protease activity and/or expression have been identified in patients with cerebral autosomal recessive arteriopathy with subcortical infarcts and leukoencephalopathy (CARASIL) (17). While there have been few reported ocular phenotypes in these patients, they exhibit cerebral small vessel arteriopathies characterized by loss of vascular smooth muscle cells, hyaline degeneration of the tunica media, and reductions in ECM proteins including type I, III, and VI collagen and fibronectin in the arterial adventitia (17, 18). In *Htra1* knockout mice, cerebral arteries appeared normal, but proteomic analysis of protein extracts derived from cerebral vessels demonstrated an increase in levels of many extracellular proteins including Timp3, fibulin 3 (encoded by *Efemp1*), elastin, vitronectin, and clusterin, suggesting they are candidate substrates of HtrA1 that accumulate in its absence (19). Conversely, transgenic mice overexpressing human *HTRA1* in the RPE showed fragmentation of the elastin layer of BM and decreased levels of tropoelastin and fibulin 5 in lysates from the RPE-choroid (20, 21). Collectively, these results demonstrate that HtrA1 likely plays a key role in maintaining the integrity of vascular walls and/or structural membranes rich in collagens, elastin, and ECM proteins. Loss of HtrA1 protein expression or activity may impair the normal functions of these structures.

The objective of the current study was to identify mechanisms responsible for the increased susceptibility for AMD associated with the 10q26 risk haplotype. Employing a large repository of human donor eyes, we showed that *HTRA1* messenger RNA (mRNA) and protein expression were higher in RPE-choroid tissue from aged donors with homozygous nonrisk haplotype combinations (diplotypes) as compared to donors with homozygous risk diplotypes. This elevated expression of *HTRA1* was associated with a cis-acting DNA regulatory element within a ~4-kb region in the AMD-associated 10q26 locus, refined by using tissues derived from donors with recombinant haplotypes. The ability of this *HTRA1* regulatory region to promote *HTRA1* mRNA expression was impaired in RPE tissue from donors with Chr10 risk, as shown by reduced levels of *HTRA1* in RPE tissue from homozygous risk donors and by allele-specific expression (ASE) of *HTRA1* in RPE tissue derived from heterozygous donors. The chromatin within the *HTRA1* regulatory region was accessible and exhibited epigenetic marks consistent with an enhancer element in RPE tissue. In vitro studies showed that the risk allele at rs36212733 impaired the ability of Lhx2 protein to bind a consensus DNA binding site sequence found within the *HTRA1* regulatory region, suggesting one possible mechanism for reduced *HTRA1* expression. Finally, immunohistochemical (IHC) analyses showed high levels of HtrA1 in the sub-RPE space, proximal to BM, in tissue samples derived from nonrisk donors; levels were significantly reduced in samples derived from homozygous risk donors. Collectively, these results indicate that the failure to express *HTRA1* at sufficient levels at the RPE-Bruch's interface in individuals carrying one or two risk alleles may underlie early events in the AMD disease process. *HTRA1* augmentation, rather than removal or inhibition of HtrA1, may result in a meaningful therapeutic benefit for the treatment of chromosome 10-directed AMD.

Results

Decreased *HTRA1* mRNA Expression in RPE. To better understand the association between 10q26 genotypes and AMD etiology, we examined mRNA expression of the *ARMS2* and *HTRA1* genes in human ocular tissues, comparing age-matched donors with homozygous risk (TT), heterozygous risk (GT), and nonrisk (GG) diplotypes at the 10q26 locus based upon the rs10490924 SNP. Importantly, these analyses were performed with tissues derived

from human donors without clinical diagnoses of AMD or postmortem evidence of AMD-associated pathology and without any risk at chromosome 1q32, the *CFH*-associated AMD risk locus. This was done to identify Chr10-driven molecular changes that contribute to AMD disease initiation and/or early progression, while excluding changes driven by genetic risk at Chr1. qRT-PCR analyses showed a significant decrease in *HTRA1* mRNA transcript levels in the extramacular RPE-choroid tissue of homozygous risk ($P < 0.0001$) and heterozygous risk donors ($P = 0.0004$), as compared to homozygous nonrisk donors (Fig. 1A). These differences in *HTRA1* expression between genotype groups were not observed in extramacular retina (Fig. 1B). *HTRA1* mRNA expression did not change significantly with age in the neural retina or RPE-choroid derived from donors between 60 and 90 y of age (Fig. 1C and D). Gene expression analyses, using a custom microarray, confirmed that *HTRA1* mRNA was decreased in both the extramacular and macular RPE-choroid tissue samples derived from donors heterozygous or homozygous for 10q26 risk relative to tissue samples from donors without risk. Similar to the qRT-PCR results above, levels were not reduced in retina tissue samples from these same homozygous risk donors (Fig. 1E and *SI Appendix, Fig. S1*). Microarray analyses also demonstrated that *HTRA1* was the most significant differentially expressed gene ($P = 5.62 \times 10^{-5}$ after Bonferroni correction) in extramacular RPE-choroid tissue, with ~30% less expression in homozygous risk tissue samples, as compared to homozygous nonrisk samples. *ARMS2* expression was not detected in either tissue by qRT-PCR or microarray analysis when using human donor ocular tissue as the source of mRNA.

To examine whether *HTRA1* levels are reduced in RPE-choroid tissue from donors with AMD and Chr10 risk when compared to donors without AMD or Chr10 risk, we reanalyzed previously published microarray data (22) in which the donor samples were subsequently genotyped. Donor tissues in this cohort were originally selected based upon AMD status but not upon genetic risk at either Chr1 or Chr10. As a result, most donors with risk at the Chr10 locus were heterozygotes, and many also carried risk alleles at the Chr1 locus. Despite this, *HTRA1* mRNA was significantly reduced in the extramacular RPE-choroid tissue of donors with AMD and heterozygous risk at Chr10 ($n = 16$) versus tissue from donors without AMD and no risk at Chr10 ($n = 16$) ($P = 0.0045$) (*SI Appendix, Fig. S2*). In macular RPE-choroid, there was a statistically significant difference ($P = 0.021$) between these groups only if donors with late-stage disease were excluded (*SI Appendix, Fig. S2*), likely because of extensive RPE cell loss in the macula in late-stage disease. Significant differences in *HTRA1* expression were only observed when comparing nonrisk to risk genotype groups, indicating that reduced levels are determined by genotype status and not AMD status. This highlights the fact that the 10q26 locus increases risk for AMD but that other age-related and genetic factors can promote disease development.

***HTRA1* ASE.** To more definitively demonstrate that the Chr10 risk haplotype confers reduced *HTRA1* mRNA expression, we measured the ratio of nonrisk and risk alleles at rs1049331, a 10q26 risk SNP lying within *HTRA1* exon 1, by digital droplet PCR. By using genomic DNA (gDNA) and mRNA-derived complementary DNA (cDNA) from retina and RPE-choroid of heterozygous donors, subtle quantitative differences can be measured with high sensitivity because the ratio of both alleles is measured in the same reaction, independent of absolute levels of *HTRA1* DNA or mRNA. As expected, gDNA from heterozygous donor tissues exhibited a 50:50 ratio for the two alleles (Fig. 2A). There was a similar 50:50 ratio of the two alleles in mRNA-derived cDNA from retina tissue samples of heterozygous donors. In stark contrast, there was a significant reduction ($P < 0.0001$) in the risk allele, relative to the nonrisk allele, in mRNA-derived cDNA from RPE-choroid tissue of the same heterozygous donors. This resulted in an ~60:40 ratio for nonrisk- to risk-encoded mRNA

levels in heterozygous tissue samples (Fig. 2A). In an independent cohort of donor tissue samples in which RPE was separated from choroid, only RPE exhibited ASE of *HTRA1*, with a median ratio of ~65:35 nonrisk- to risk-encoded *HTRA1* mRNA. This was statistically different from the ratio observed in retina ($P < 0.0001$)

and choroid ($P < 0.0001$) tissue samples from the same donor cohort (Fig. 2B).

To further refine the region responsible for reduced *HTRA1*, ocular tissues from human donors with rare recombinant haplotypes within the 10q26 region were utilized in the ASE assay

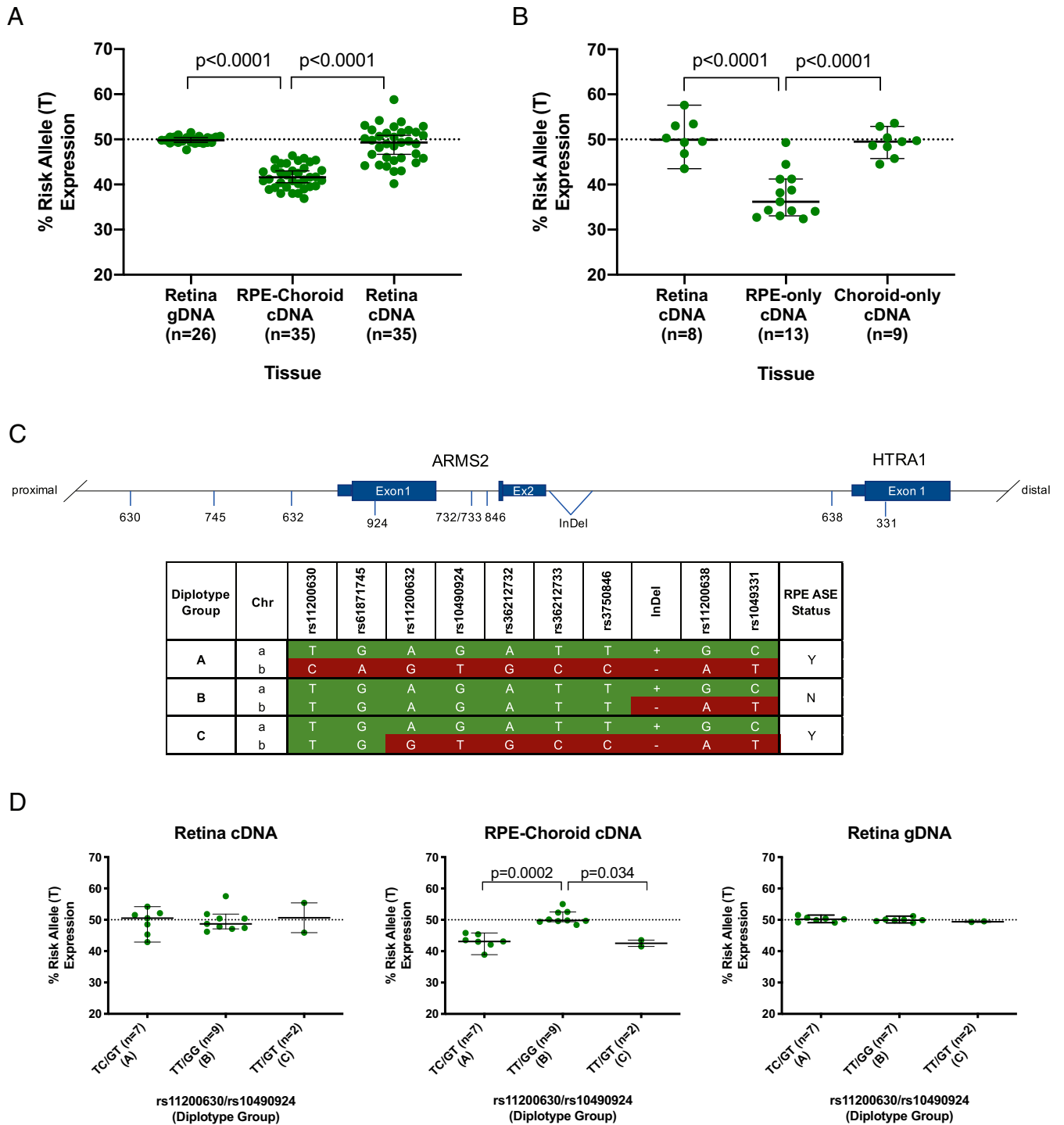


Fig. 2. *HTRA1* allele-specific mRNA expression in human donor tissues heterozygous at coding SNP rs1049331. For each donor tissue sample, the percentage of *HTRA1* mRNA-derived cDNA or gDNA with the risk (T) allele at rs1049331 was determined. (A and B) ASE analysis using RNA or control gDNA derived from donor retina and RPE-choroid tissue samples (A) or from donor retina, RPE-only and choroid-only tissue samples (B). (C) Schematic of the recombinant diplotype groups at the Chr10 locus. (D) *HTRA1* ASE analysis using mRNA-derived cDNA or control gDNA from retina and RPE-choroid tissue samples from donors with the recombinant diplotype groups presented in C. The dashed line in the graphs marks the expected 50:50 ratio of the nonrisk and risk alleles if there were no ASE of *HTRA1*. Median values with 95% CI are shown. Mann-Whitney *U* test analysis was used to determine significance.

(Fig. 2C). Relative to heterozygous donors (diplotype group A), donors in diplotype groups B and C were homozygous nonrisk in a portion of the chromosome 10q26 block proximal to the indel that lies between the *ARMS2* and *HTRA1* genes (group B) or proximal to rs11200632, which lies upstream of the *ARMS2* gene (group C). The ASE of *HTRA1* seen in RPE-choroid samples from heterozygous diplotype group A is lost in diplotype group B but not in diplotype group C (Fig. 2D). This implies that one or more SNPs within a ~4-kb region lying between and including rs11200632 and rs3750846 and that overlaps exon 1 and a portion of intron 1 of the *ARMS2* gene is causally associated with the RPE-specific reduction in *HTRA1* expression. This region is herein referred to as the “*HTRA1* regulatory region.”

HTRA1 Protein Expression in Human Ocular Tissues. To evaluate whether reduced *HTRA1* mRNA levels in RPE tissue samples derived from homozygous risk donors translates into reduced protein levels, we quantified HtrA1 protein in the RPE-choroid and retina from age-matched donors using enzyme-linked immunosorbent assay (ELISA) (Fig. 3A–F). HtrA1 protein concentrations were reduced ~50% in tissue samples from RPE-choroid (Fig. 3A) but not retina (Fig. 3B) when comparing all homozygous risk samples to all nonrisk samples ($P = 0.0094$). Interestingly, there was an age-dependent increase in HtrA1 protein levels in

RPE-choroid tissue samples derived from homozygous nonrisk donors but not those from homozygous risk donor samples ($P = 0.033$) (Fig. 3E). As a result, the median concentration of HtrA1 protein in nonrisk donors (34.5 ng/mg) was threefold higher than in risk donors (12.3 ng/mg) when comparing only those donors over age 65 (Fig. 3C). In contrast, levels of HtrA1 protein remain constant with age in retina samples regardless of Chr10 risk status (Fig. 3F) and show no significant difference when comparing genotype groups (Fig. 3B and D). Quantification of HtrA1 protein from retina, RPE only, BM only, and BM with choroid (BM-Ch) derived from both macular and extramacular regions of homozygous nonrisk donor eyes indicates that HtrA1 is highly enriched in BM-containing extracts. Macular BM-choroid extracts had significantly higher levels of HtrA1 than the extramacular BM-choroid extracts ($P = 0.0010$), suggesting that HtrA1 may be particularly important in this region (SI Appendix, Fig. S3). Immunohistochemical analyses of tissue from a homozygous nonrisk donor showed that HtrA1 staining was most intense in the sub-RPE space along BM, in retinal arteries and in the outer aspect of the retinal inner nuclear layer, consistent with the location and density of horizontal cells (Fig. 3G and SI Appendix, Fig. S4), which are known to express high levels of *HTRA1* mRNA (23, 24). There was also intense staining of hard drusen lying between the RPE and BM (Fig. 3H), as previously shown (25). When comparing HtrA1

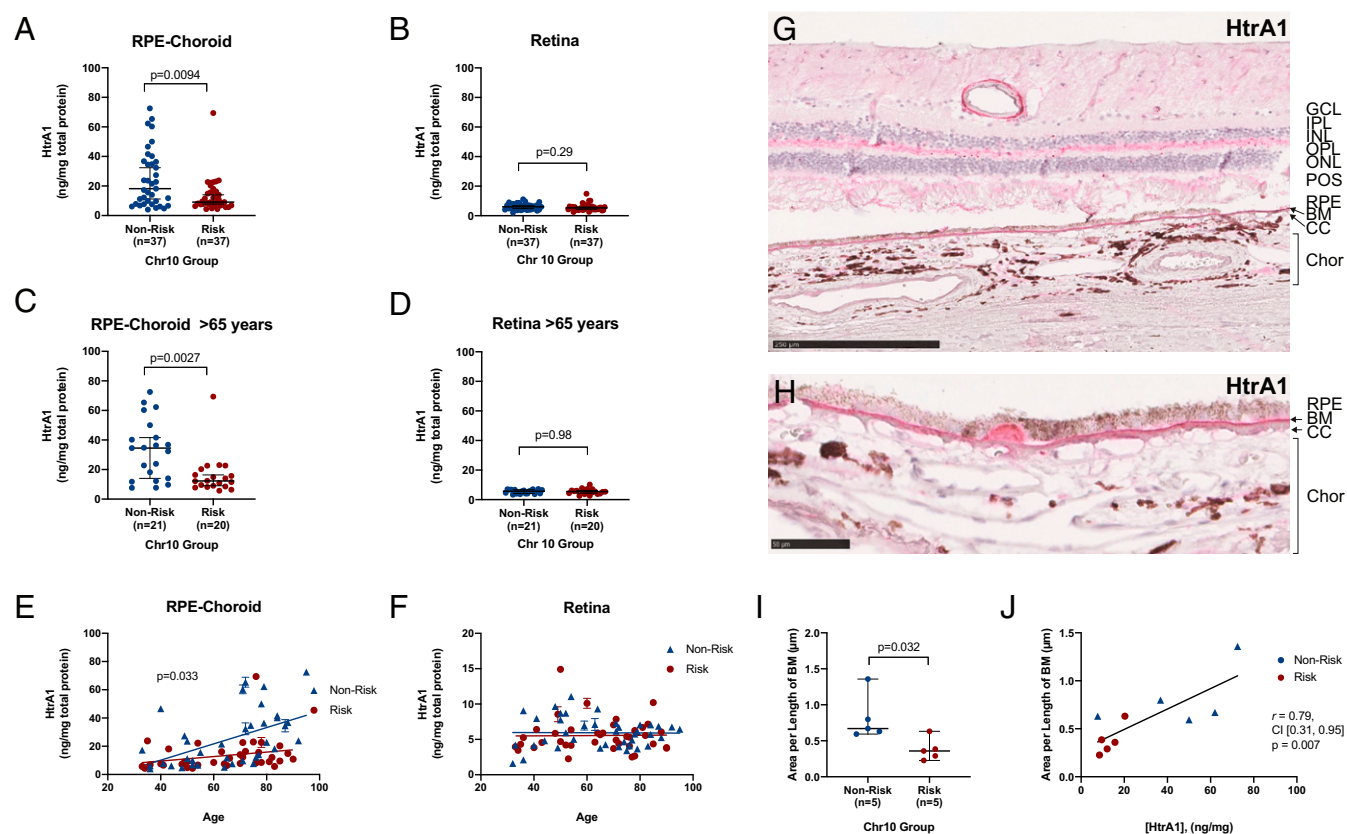


Fig. 3. Analyses of HtrA1 protein in human donor ocular tissues. (A–D) ELISA analysis of total HtrA1 protein concentration in RPE-choroid (A and C) or retina (B and D) tissues from donors of all ages (A and B) or in donors over 65 (C and D), comparing homozygous nonrisk or risk genotype groups. Median values with 95% CI are shown. Mann–Whitney *U* test analysis was used to determine significance. (E and F) Concentrations of HtrA1 in each genotype group were also plotted by donor age for RPE-choroid (E) and retina (F). The *P* value in E indicates the slope of the two lines are significantly different. (G and H) HtrA1 immunohistochemistry in retina and RPE-choroid tissues from a homozygous nonrisk donor using anti-HtrA1 antibody NEP-2717 and warp red chromagen. Upper image (G) shows intense staining of HtrA1 in retina artery, outer aspect of inner nuclear layer, and in BM. Lower image (H) is a higher magnification, highlighting the presence of HtrA1 in BM and drusen-like deposits (marked with asterisk). Scale bars represent 250 μm in Upper image and 50 μm in Lower image. (I) Quantitation of IHC HtrA1 staining within a 10- μm -wide region along BM in homozygous nonrisk and risk donor tissue ($n = 10$). Each dot represents the average from two slide sections from each donor, and the values represent the HtrA1-positive surface area per length of BM ($\mu\text{m}^2/\mu\text{m}$). Mann–Whitney *U* test analysis was used to determine significance. (J) Pearson correlation of HtrA1 protein concentration determined by ELISA relative to surface area of HtrA1 staining at BM from the same donors ($n = 10$) as shown in I.

staining in the sub-RPE space using digitized, segmented IHC images of donor tissue with and without Chr10 risk (*SI Appendix, Fig. S5*), HtrA1 staining was significantly reduced in risk tissue samples ($P = 0.032$) (Fig. 3). Importantly, the HtrA1 protein signal at BM of fixed eyes correlated strongly with the HtrA1 protein concentrations measured by ELISA analyses of the RPE-choroid derived from the contralateral flash-frozen eyes from the same donors ($r = 0.79$, CI [0.31 to 0.95], $P = 0.007$) (Fig. 3). This implies that a majority of the HtrA1 signal in RPE-choroid protein extracts is derived primarily from BM.

Characterization of the RPE-Specific *HTRA1* Regulatory Region. We hypothesized that the 4-kb *HTRA1* regulatory region might contain an RPE-specific enhancer that functions to increase *HTRA1* mRNA expression and that one or more risk-associated SNPs within the region impairs this enhancer function. Liao et al. (26) previously reported a region of open chromatin within the *ARMS2* intron in RPE cells; this was further supported by assay for transposase-accessible chromatin with sequencing (ATAC-Seq) data from fetal RPE (fRPE) and induced pluripotent stem cell-RPE (iPS-RPE) cell models (*SI Appendix, Fig. S6*). To investigate further, we performed chromatin immunoprecipitation and sequencing (ChIP-Seq) experiments employing antibodies targeting epigenetic marks associated with enhancer elements, including acetylated lysine 27 (H3K27Ac) and monomethylated lysine 4 (H3K4me1) on histone 3, using retina and RPE tissues derived from homozygous nonrisk adult human donors. In RPE tissue, we identified a statistically significant H3K27Ac peak that overlaps the 4-kb *HTRA1* regulatory region on Chr10 and is centered upon the open chromatin region in *ARMS2* (Fig. 4A and *Dataset S1*), in agreement with H3K27Ac ChIP-Seq data from both fRPE and iPS-RPE cells (*SI Appendix, Fig. S6*). This peak was only present in RPE-enriched tissue and was not observed in the neural retina (Fig. 4B and *Dataset S1*). A peak centered on the *ARMS2* intron region was also observed in the H3K4me1 ChIP-Seq analyses for both retina and RPE tissue (Fig. 4A and B and *Dataset S2*). The presence of an ATAC-Seq signal in conjunction with H3K4me1 and H3K27Ac epigenetic marks in RPE tissue suggests that the region within the *ARMS2* intron is an active tissue-specific enhancer element.

A previous study showed that the Otx2 transcription factor can bind to the *HTRA1* regulatory region in retina (*SI Appendix, Fig. S7*) (27). We performed Otx2 ChIP-seq analysis, comparing retina and RPE from a single donor. We showed that Otx2 binds the intronic region of *ARMS2* within the *HTRA1* regulatory region in both retina and RPE (*SI Appendix, Fig. S7* and *Dataset S3*) but does not bind sites within the *HTRA1* intron 1 or exon 6 in RPE. These results support the hypothesis that the *HTRA1* regulatory region may function as a transcriptional enhancer element for *HTRA1* expression and that expression of *HTRA1* is differentially regulated in retina versus RPE. An Otx2 consensus binding motif (GGATTA) is located within the *ARMS2* intron in the region bound by Otx2, but it does not overlap any of the AMD-associated SNPs. Thus, we performed bioinformatic analyses to identify transcription factors whose consensus binding motif overlaps the AMD-associated SNPs within this enhancer element and which potentially exhibit differential binding between nonrisk and risk alleles. Factors whose binding site overlaps rs36212733 included *Lhx2*, *Pou6f1*, *Znf333*, *Vsx2*, and *Alx1/3*. Of these candidates, only *LHX2* mRNA is expressed at modest levels in RPE tissues, whereas the other factors are low or absent, as determined by RNA-Seq (*SI Appendix, Fig. S8* and *Dataset S4*). Attempts to perform ChIP-Seq analysis of Lhx2 binding in RPE tissue were unsuccessful, possibly due to the modest levels of *LHX2* expression in RPE, the limited number of RPE cells available from any given donor eye, and/or inadequate antibodies available for ChIP-Seq. Instead, electrophoretic mobility shift assays (EMSA) were performed to assess whether Lhx2 protein binds to Chr10 nonrisk or risk DNA sequences. Nuclear extracts from HEK293 cells

transfected with plasmid encoding *LHX2* were employed with biotinylated oligo probes containing nonrisk or risk alleles at the SNPs rs36212732 and rs36212733. The risk allele at rs36212733 SNP disrupts one of the critical residues within the Lhx2 binding motif by converting the “T” at position 6 to a “C” (Fig. 4C). Oligo probes containing the scrambled sequence of this region (SCR, negative control) or a previously reported Lhx2 binding motif sequence (POS, positive control) (28) were also included in these experiments (*SI Appendix, Fig. S9*). A protein from nuclear extracts containing overexpressed Lhx2 but not empty vector bound to both the nonrisk and risk probes, as well as to the positive control probe (red asterisk) but not to the scrambled probe (Fig. 4D and *SI Appendix, Fig. S9*). Addition of an anti-Lhx2 antibody to the EMSA reaction resulted in a supershift of the Lhx2 band (marked with green asterisk), confirming that this band corresponded to Lhx2 (Fig. 4D). Competition studies adding unlabeled nonrisk probe resulted in loss of the Lhx2 band and several others which may represent other nuclear proteins capable of binding the oligo probe sequence (Fig. 4D). Binding of Lhx2 to the nonrisk probe increased as the amount of biotinylated DNA probe in the reactions was increased from 10 to 80 fmoles. In contrast, Lhx2 only weakly bound the risk probe at all concentrations (Fig. 4E). Overall, these results show that Lhx2 can bind to the DNA probe encompassing the rs36212733 nonrisk SNP and that its ability to bind the DNA probe with the risk rs36212733 SNP is significantly compromised.

Discussion

This study provides a comprehensive analysis of *HTRA1* mRNA and protein expression in human ocular tissues derived from a large cohort of age-matched donor tissue samples, comparing the AMD-associated 10q26 nonrisk and risk genotype groups. Our findings demonstrate that HtrA1 protein levels increase significantly with age in the RPE-choroid of homozygous nonrisk donors and that *HTRA1* mRNA and protein expression is reduced in the RPE of homozygous risk donors relative to homozygous nonrisk donors. Reduced expression of *HTRA1* occurred in RPE tissues from donors without AMD, suggesting that this is an early event in the disease process. These observations contradict published literature that reports either no difference or elevated expression of *HTRA1* in retina tissue derived from donors with 10q26 risk (25, 29–31). In those studies, few samples were employed, and/or the analyses were performed using neural retina or white blood cells rather than RPE or RPE-choroid tissue. Given the broad range of *HTRA1* mRNA and protein expression in ocular tissues from nonrisk donors (Figs. 1 and 3), large sample sizes for both homozygous nonrisk and risk donor tissue samples are required to determine statistically significant differences in expression. Furthermore, since HtrA1 protein expression increases with age in nonrisk donors, it is imperative that the donor tissue cohorts are appropriately matched for age. Our data indicate that the *HTRA1* regulatory region is an RPE tissue-specific enhancer element and thus other tissues or cell types may not be a reliable substitute for measuring the effect of the risk alleles on *HTRA1* expression.

By measuring allele-specific *HTRA1* mRNA expression in tissues from donors with recombinant haplotypes, we identified a ~4-kb region that influences the expression of *HTRA1*. This region is nearly identical to the one identified by Grassmann et al. (9) as being associated with elevated risk of AMD based on case-control studies of AMD patients with recombinant haplotypes. This region contains 12 variants in and immediately upstream of *ARMS2* but does not contain the *ARMS2* indel, the *HTRA1* promoter SNP (rs11200638), or the silent SNPs (rs1049331 and rs2293870) lying within *HTRA1* exon 1, all of which were previously reported to be causal variants in 10q26 for elevated AMD risk (10, 25, 32). Combined, these data support the hypothesis that risk variants within the *HTRA1* regulatory region lead to both reduced expression of *HTRA1* and elevated risk of AMD, thereby providing a molecular mechanism that links the

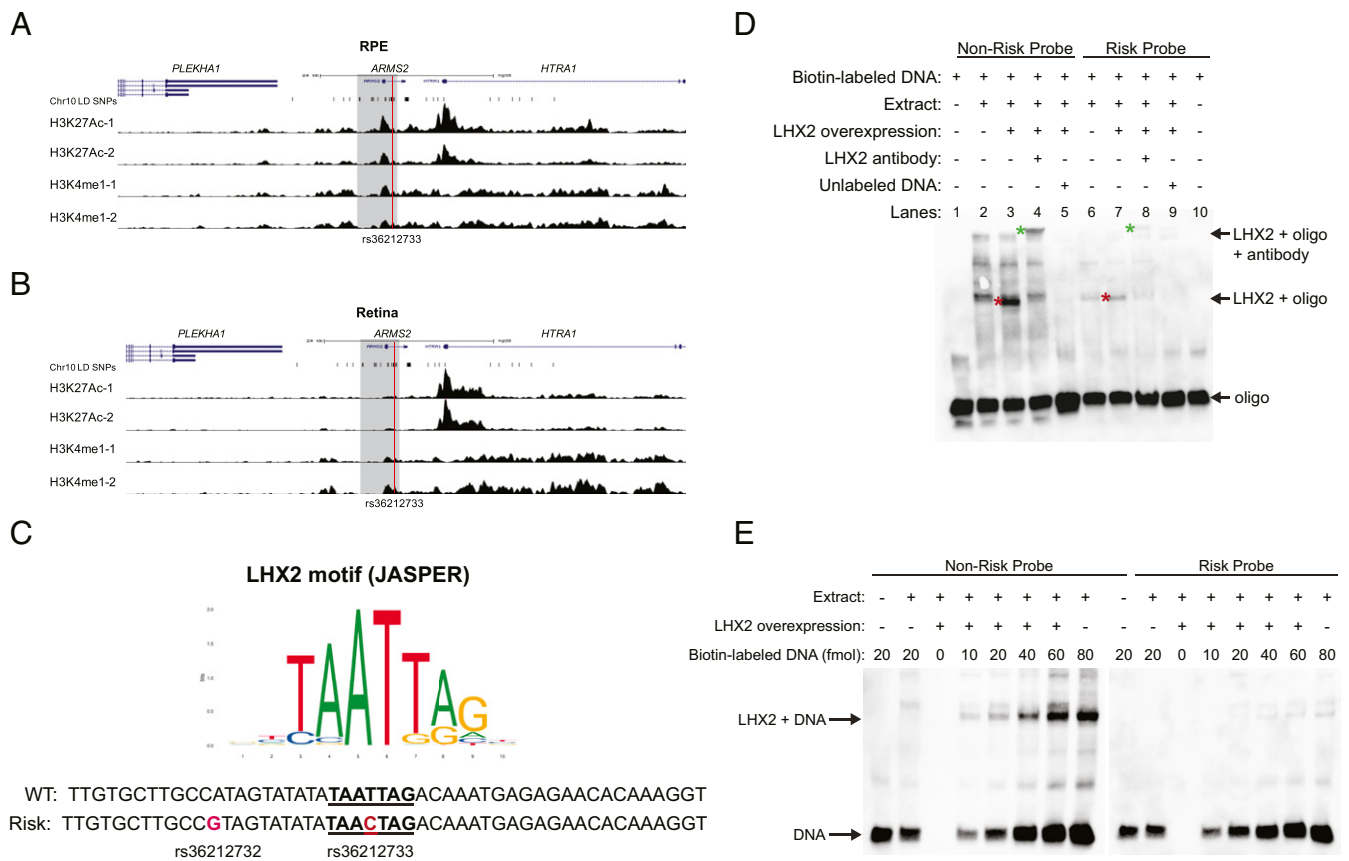


Fig. 4. Epigenetic analysis of Chr10 AMD-associated locus. (A and B) ChIP-Seq analysis of H3K27Ac and H3K4me1 in adult human RPE (A) or retina (B) tissue from two independent homozygous nonrisk donors (-1 and -2). Normalized fragment coverage is displayed. The gray region represents the 4-kb *HTRA1* regulatory region, and the red line marks the location of rs36212733. (C) Consensus Lhx2 DNA binding motif and predicted Lhx2 binding site (underlined) within the 4-kb *HTRA1* regulatory region on Chr10 overlapping the rs36212733 SNP. (D) EMSA analysis for SNP-genotype-specific binding of nuclear extracts from HEK293 cells with (+) or without (-) transient Lhx2 overexpression to oligonucleotide (oligo) probes with the risk or nonrisk SNPs at rs36212732 and rs36212733. Anti-Lhx2 antibody or unlabeled probe was included in some reactions, as indicated. Red asterisk indicates band found in Lhx2-containing nuclear extracts but not extracts without Lhx2 overexpression. Green asterisk indicates the band supershifted with addition of Lhx2 antibody to the reaction. (E) Same as in D, except that increasing amounts of biotin-labeled probe were included in the reaction mixture.

chromosome 10q26 risk genotype to the AMD phenotype. We show that the *HTRA1* regulatory region has the signature features of an active enhancer element in RPE tissue and provide plausible evidence that the Lhx2 transcription factor can bind a motif that overlaps rs36212733 and that binding is impaired by the risk allele at this motif. We were unable to detect ASE of *HTRA1* mRNA using several RPE model systems, including differentiated human fRPE cells from three different donors, two independent iPS-RPE cell models, and two RPE cell lines (ARPE19 and hRPE7). A third RPE cell line, hTERT-RPE1, exhibited ASE of *HTRA1*, but genomic copy number analysis revealed that this cell line has an extra nonrisk copy of the 10q26 locus. Thus, it was unclear whether the altered expression of *HTRA1* mRNA was a consequence of ASE or due to abnormal duplication of the 10q26 region. RPE models do not fully express the same repertoire of genes found in adult RPE tissue, and interactions with the surrounding tissues may be required to drive the expression of these genes (33–36). Without an in vitro cell culture model system in which the *HTRA1* regulatory region is functioning as an RPE-specific active enhancer, we were unable to directly show, via gene-editing methods, that modifying the rs36212733 SNP, the *HTRA1* regulatory region, or the *LHX2* gene results in decreased *HTRA1* expression. As such, Lhx2 is a candidate regulator of RPE-specific *HTRA1* expression via binding to the nonrisk variant at rs36212733. It remains possible that other variants within the open chromatin

region of the *HTRA1* regulatory region play a role in regulating *HTRA1* expression and/or that other RPE-specific factors are required for activation of this enhancer element.

IHC analyses showed a strong accumulation of HtrA1 protein at the RPE–BM interface of nonrisk donors. The permeability and hydraulic conductivity of BM decreases with age due to the accumulation of lipids and oxidized biomolecules that are waste products of RPE metabolism (3). Given the higher-order multimeric structures formed by HtrA1 monomers (37), it is unlikely that these complexes are capable of crossing aged BM from the choroidal aspect, suggesting that RPE is the primary source of HtrA1 located within the sub-RPE space. HtrA1 functions as both a serine protease and an extracellular chaperone protein. It solubilizes protein aggregates and proteolytically degrades substrates (38), many of which are ECM proteins and structural components of BM and RPE basal lamina, including elastin, nidogen 2, aggrecan, decorin, fibromodulin, collagen VI, and fibronectin (21, 39). AMD is characterized by the accumulation of membranous debris and protein aggregates that include ECM proteins such as TIMP3 and vitronectin (40, 41) in the sub-RPE space. Evidence suggests that long-spacing type VI collagen and ECM proteins are key components of basal laminar deposits, a common pathological feature of AMD (42). A failure to produce sufficient amounts of HtrA1 protein to process/degrade these aggregates may result in their accumulation. Interestingly, AMD-like diseases such as

Sorsby's fundus dystrophy, late-onset retinal dystrophy, and Doyme honeycomb retinal dystrophy (Malattia leventinese) are caused by mutations in genes encoding ECM proteins, including *TIMP3*, *ClqTNF5* (*CTRP5*), and *EFEMP1*, respectively. All three diseases result in the accumulation of basal laminar deposit-like material in the sub-RPE space (43). We propose that HtrA1 protein functions to maintain optimal proteostasis of BM. Disruption of this balance may occur due to decreased HtrA1 protein in Chr10-directed AMD or to increased levels of mutated, mis-folded ECM proteins in AMD-like diseases. These disturbances promote the accumulation of damaged proteins, which ultimately leads to the formation of drusen and/or basal laminar deposits and to impaired function and integrity of the RPE, the choriocapillaris, and the outer retinal layers, elevating the risk for AMD.

Additional support for decreased level and activity of HtrA1 protein associated with human disease is exemplified by individuals with CARASIL or cerebral autosomal dominant arteriopathy with subcortical infarcts and leukoencephalopathy (CADASIL). In CARASIL patients, autosomal-recessive mutations in *HTRA1* result in decreased expression or activity, leading to cerebral artery pathologies (17, 18, 44). In CADASIL patients, autosomal-dominant mutations in *NOTCH3* lead to the formation of intermolecular aggregates and accumulation of protein deposits in the tunica media of small cerebral arteries (45, 46). These deposits were shown by proteomic analyses to contain various ECM structural proteins and modifying enzymes, including HtrA1 (19). Many of the same ECM proteins found in deposits of CADASIL patients are also elevated in the vasculature of *Htra1* knockout mice, suggesting that in CADASIL patients, HtrA1 is functionally sequestered in these deposits, which then allows for the accumulation of its substrates in the vessel walls (19). Interestingly, some of the proteins that accumulate in the vessels of CADASIL patients or *Htra1* knockout mice include fibulin 3 (*EFEMP1*), *Timp3*, and members of the *Clqtnf* family, providing evidence that turnover of these proteins in the ECM may be regulated by HtrA1 activity, either directly or indirectly. These are the same genes that are mutated in the AMD-like diseases described above. Thus, analogous to RPE tissue with homozygous Chr10 risk, deficient expression or activity of HtrA1 in the cerebral vasculature of CARASIL and CADASIL patients impairs or overwhelms the ability of HtrA1 to maintain optimal proteostasis of the ECM in the vascular walls of cerebral arteries. While individuals with CADASIL can exhibit ocular phenotypes (47, 48), few have been reported in individuals with CARASIL, although the life expectancy of these individuals rarely exceeds the sixth decade. This is consistent with the notion that risk alleles at the 10q26 locus increase the risk of AMD but that other genetic and age-related factors may be required for the disease to manifest fully.

Overall, our results demonstrate that the chromosome 10q26 risk alleles associated with AMD drive RPE-specific and age-dependent reductions in *HTRA1* gene expression via a 4-kb regulatory region overlapping a portion of the *ARMS2* gene. Reduced levels of HtrA1 protein during the aging process may disrupt the integrity of BM and RPE function, leading to increased risk of pathological consequences including RPE cell detachment and death, geographic atrophy, and/or choroidal neovascularization. Experiments are in progress to develop a nonhuman primate model to examine whether reduced expression of *HTRA1* in the RPE, in combination with treatments that mimic the aging process, lead to phenotypes consistent with AMD, such as the accumulation of basal laminar deposits, drusen formation, and/or RPE and choriocapillary endothelial cell death. If supported, it would indicate that restoration of *HTRA1* expression, rather than removal or inhibition of HtrA1 activity, may provide meaningful therapeutic benefit for the treatment of chromosome 10-directed AMD.

Materials and Methods

Human Ocular Tissue Collection. This study was reviewed and approved by the institutional review board at the University of Utah and conforms to the tenets of the Declaration of Helsinki. Written informed consent was obtained from the surviving relatives of all human eye donors or by the donors prior to time of death. Neural retina and RPE-choroid samples were isolated from human donor eyes obtained from the Lions Eye Bank of Utah. Eyes were collected within 5 h of the time of death. Upon receipt, the anterior portion of the eye was removed, and four parallel incisions were made to flat mount the eye. An 8-mm trephine punch of the macula and 6-mm trephine punch of the temporally adjacent extramacular region were obtained, and the retina and RPE-choroid layers were separated from one another prior to flash freezing in liquid nitrogen.

Sample Genotyping. gDNA was isolated from peripheral blood leukocytes, and genotyping was performed using predesigned Taqman assays (Applied Biosystems).

RNA Isolation from Eye Tissue. Tubes containing frozen neural retina or RPE-choroid tissue were placed in a dry ice/ethanol slurry and ground to a fine powder while still frozen. Upon transferring to ice, RLT lysis buffer from the Qiagen AllPrep kit was added to the sample and, following a second grinding, was further homogenized by passage through a QIAshredder column (Qiagen). DNA, RNA, and protein were purified from the flow-through using an AllPrep kit (Qiagen) per the manufacturer's protocol. A second DNase I treatment was performed on all RNA samples. RNA integrity was measured using the Agilent Bioanalyzer RNA 6000 Pico chip assay. RNA concentration was determined using a nanodrop spectrophotometer. Additional methods for isolating RNA from isolated RPE and choroid are described in the *SI Appendix*.

qRT-PCR. First strand cDNA synthesis was performed with 100 ng RNA using the ThermoScript RT-PCR kit (Thermo Fisher Scientific). Approximately 20 to 100 ng first strand product was used as template for qPCR. qPCR was performed with the 2X RT² SYBR Green ROX qPCR mastermix and primers specific for *HTRA1* (qHsaCID0016596, BioRad) and *GAPDH* (qHsaCED0038674, BioRad). The qPCR reactions were performed in duplicate on an Applied Biosystems 7500 RT-PCR instrument using standard PCR conditions. All Ct values were normalized to the *GAPDH* reference gene and plotted as fold increase relative to the average of all samples using the $2^{-\Delta\Delta Ct}$ method.

Ocular Tissue Protein Extraction. Tissue proteins were extracted in tissue protein extraction reagent (T-PER) lysis buffer containing 1% Halt protease and phosphatase inhibitor mixture with ethylenediaminetetraacetic acid (EDTA). After tissue homogenization with a probe sonicator, insoluble material was removed by centrifugation and the protein concentrations of the soluble supernatants were determined using the Pierce 660-nm protein assay kit (Thermo Fisher Scientific). Additional methods for extracting protein from individual ocular layers are described in the *SI Appendix*.

***HTRA1* Allele-Specific Expression Assay.** RNA (~200 ng) from human eye tissues were used as template for reverse transcription using the SuperScript IV First-Strand Synthesis kit (Thermo Fisher Scientific) and the *HTRA1* gene-specific R6 primer (R6:GGGCGATCTTCTCCACCAG). Approximately 20 ng cDNA product or 20 ng gDNA was used as template for PCR. A master mix containing 300 nM of each primer (F6:AGAGTCGCCATGCAGATCC and R4:TGGCGCACACAGAGGC) and 2X FailSafe buffer J master mix (Illumina) was added to the template. Seven cycles of PCR were performed with a 61 °C annealing temperature. A second round of nested PCR was performed using 5 μ l product from the first round and the custom Taqman SNP assay for rs1049331 (*SI Appendix*, Table S1). PCR was performed using the Type-It Fast SNP PCR master mix (Qiagen) on the RainDance RainDrop digital droplet PCR system. The percentage of droplets with a 2'-chloro-7'-phenyl-1,4-dichloro-6-carboxy-fluorescein (VIC) versus a 6-carboxyfluorescein (FAM) fluorescent signal was quantified using the RainDrop software package.

HtrA1 ELISA. Standard sandwich ELISAs were performed using HtrA1-specific NEP-2717 polyclonal antibody for capture and B18 monoclonal anti-HtrA1 antibody for detection, followed by horseradish peroxidase (HRP)-conjugated goat anti-mouse IgG antibody (Jackson ImmunoResearch). HtrA1 antibody generation and characterization along with full details of the ELISA are described in the *SI Appendix*.

HtrA1 Immunohistochemistry. Donor eyes were fixed in 4% paraformaldehyde, and an ~1-cm-wide strip encompassing the macular region was embedded in

paraffin by standard protocols. Two 5- μ m sections from each donor were stained with anti-HtrA1 (NEP-2717) antibody using standard procedures. In some cases, pairs of nonrisk and risk donor tissue were mounted on the same slide so that a comparison in HtrA1 levels could be made between the two donors under identical staining conditions. Additional details as well as methods for quantifying the signal are provided in the *SI Appendix*.

Lhx2 EMSA. Nuclear extracts from HEK293 cells overexpressing Lhx2 were prepared using the NE-PER Nuclear and Cytoplasmic Extraction Reagent kit (Thermo Fisher Scientific). Complementary biotinylated DNA oligo pairs (*SI Appendix, Table S1*) were annealed in buffer (10 mM Tris HCl, pH 7.5, 50 mM NaCl, 1 mM EDTA at 100 μ M). A binding reaction was prepared using the LightShift Chemiluminescent EMSA Kit (Thermo Scientific). Protein-DNA complexes were formed by incubating 20 fmol oligo probe with \sim 3 μ g nuclear protein extract. Supershift was performed using anti-Lhx2 antibody (Thermo Fisher Scientific, No. PA5-78287), and competition assays were performed by preincubating with unlabeled oligo probe. Additional details are provided in the *SI Appendix*.

High-Throughput Genomic Analysis. RNA-Seq and ChIP-Seq were performed according to standard published protocols. Full details are provided in the *SI Appendix*.

1. W. L. Wong *et al.*, Global prevalence of age-related macular degeneration and disease burden projection for 2020 and 2040: A systematic review and meta-analysis. *Lancet Glob. Health* **2**, e106–e116 (2014).
2. M. A. Zouache *et al.*, Macular retinal thickness differs markedly in age-related macular degeneration driven by risk polymorphisms on chromosomes 1 and 10. *Sci. Rep.* **10**, 21093 (2020).
3. I. Bhatta, G. Luttj, Understanding age-related macular degeneration (AMD): Relationships between the photoreceptor/retinal pigment epithelium/Bruch's membrane/choriocapillaris complex. *Mol. Aspects Med.* **33**, 295–317 (2012).
4. L. G. Fritsche *et al.*, A large genome-wide association study of age-related macular degeneration highlights contributions of rare and common variants. *Nat. Genet.* **48**, 134–143 (2016).
5. L. G. Fritsche *et al.*, Age-related macular degeneration: Genetics and biology coming together. *Annu. Rev. Genomics Hum. Genet.* **15**, 151–171 (2014).
6. J. Jakobsdottir *et al.*, Susceptibility genes for age-related maculopathy on chromosome 10q26. *Am. J. Hum. Genet.* **77**, 389–407 (2005).
7. G. S. Hageman *et al.*, A common haplotype in the complement regulatory gene factor H (HF1/CFH) predisposes individuals to age-related macular degeneration. *Proc. Natl. Acad. Sci. U.S.A.* **102**, 7227–7232 (2005).
8. A. Rivera *et al.*, Hypothetical LOC387715 is a second major susceptibility gene for age-related macular degeneration, contributing independently of complement factor H to disease risk. *Hum. Mol. Genet.* **14**, 3227–3236 (2005).
9. F. Grassmann, I. M. Heid, B. H. F. Weber, International AMD Genomics Consortium (IAMGDC), Recombinant haplotypes narrow the ARMS2/HTRA1 association signal for age-related macular degeneration. *Genetics* **205**, 919–924 (2017).
10. L. G. Fritsche *et al.*, Age-related macular degeneration is associated with an unstable ARMS2 (LOC387715) mRNA. *Nat. Genet.* **40**, 892–896 (2008).
11. A. Kanda *et al.*, A variant of mitochondrial protein LOC387715/ARMS2, not HTRA1, is strongly associated with age-related macular degeneration. *Proc. Natl. Acad. Sci. U.S.A.* **104**, 16227–16232 (2007).
12. E. Kortvely *et al.*, ARMS2 is a constituent of the extracellular matrix providing a link between familial and sporadic age-related macular degenerations. *Invest. Ophthalmol. Vis. Sci.* **51**, 79–88 (2010).
13. G. Wang *et al.*, Localization of age-related macular degeneration-associated ARMS2 in cytosol, not mitochondria. *Invest. Ophthalmol. Vis. Sci.* **50**, 3084–3090 (2009).
14. A. De Luca *et al.*, Distribution of the serine protease HtrA1 in normal human tissues. *J. Histochem. Cytochem.* **51**, 1279–1284 (2003).
15. G. Hansen, R. Hilgenfeld, Architecture and regulation of HtrA-family proteins involved in protein quality control and stress response. *Cell. Mol. Life Sci.* **70**, 761–775 (2013).
16. D. Zurawa-Janicka *et al.*, Structural insights into the activation mechanisms of human HTRA serine proteases. *Arch. Biochem. Biophys.* **621**, 6–23 (2017).
17. K. Hara *et al.*, Association of HTRA1 mutations and familial ischemic cerebral small-vessel disease. *N. Engl. J. Med.* **360**, 1729–1739 (2009).
18. T. Oide *et al.*, Extensive loss of arterial medial smooth muscle cells and mural extracellular matrix in cerebral autosomal recessive arteriopathy with subcortical infarcts and leukoencephalopathy (CARASIL). *Neuropathology* **28**, 132–142 (2008).
19. A. Zellner *et al.*, CADASIL brain vessels show a HTRA1 loss-of-function profile. *Acta Neuropathol.* **136**, 111–125 (2018).
20. S. Vierkotten, P. S. Muether, S. Fauser, Overexpression of HTRA1 leads to ultrastructural changes in the elastic layer of Bruch's membrane via cleavage of extracellular matrix components. *PLoS One* **6**, e22959 (2011).
21. A. Jones *et al.*, Increased expression of multifunctional serine protease, HTRA1, in retinal pigment epithelium induces polypoidal chorioidal vasculopathy in mice. *Proc. Natl. Acad. Sci. U.S.A.* **108**, 14578–14583 (2011).
22. A. M. Newman *et al.*, Systems-level analysis of age-related macular degeneration reveals global biomarkers and phenotype-specific functional networks. *Genome Med.* **4**, 16 (2012).
23. M. Menon *et al.*, Single-cell transcriptomic atlas of the human retina identifies cell types associated with age-related macular degeneration. *Nat. Commun.* **10**, 4902 (2019).

Statistical Analyses. Data analyses were performed using GraphPad Prism 8. Significant differences between sample sets were determined using non-parametric, two-tailed Mann-Whitney *U* test. The line in each figure represents the median value for that sample set and error bars represent the 95% CI. The number of independent samples in each set is indicated in the figure and each data point represents a unique individual.

Data Availability. All processed ChIP-Seq and RNA-Seq data are available within the supplemental tables of this manuscript. Unprocessed sequencing data from human donors is treated as protected health information (PHI) and cannot be made publicly available but will be made available by the corresponding author upon request.

ACKNOWLEDGMENTS. This work was supported in part by grants from the NIH (R01 EY014800, R24 EY017404), charitable donations made to the Sharon Eccles Steele Center for Translational Medicine, Voyant Biotherapeutics LLC, and an unrestricted grant from Research to Prevent Blindness, New York, NY, to the Department of Ophthalmology and Visual Sciences, University of Utah. Research reported in this publication utilized the Bioinformatics Shared Resource and High-Throughput Genomics at Huntsman Cancer Institute at the University of Utah, which is supported by the National Cancer Institute of the NIH under Award No. P30CA042014. We are grateful to the families of all the eye donors for their generous gifts, without which this work would not have been possible.

24. S. W. Lukowski *et al.*, A single-cell transcriptome atlas of the adult human retina. *EMBO J.* **38**, e100811 (2019).
25. Z. Yang *et al.*, A variant of the HTRA1 gene increases susceptibility to age-related macular degeneration. *Science* **314**, 992–993 (2006).
26. S.-M. Liao *et al.*, Specific correlation between the major chromosome 10q26 haplotype conferring risk for age-related macular degeneration and the expression of HTRA1. *Mol. Vis.* **23**, 318–333 (2017).
27. T. J. Cherry *et al.*, Mapping the cis-regulatory architecture of the human retina reveals noncoding genetic variation in disease. *Proc. Natl. Acad. Sci. U.S.A.* **117**, 9001–9012 (2020).
28. B. Muralidharan *et al.*, LHX2 interacts with the NuRD complex and regulates cortical neuron subtype determinants *Fzf2* and *Sox11*. *J. Neurosci.* **37**, 194–203 (2017).
29. C.-C. Chan *et al.*, Human HtrA1 in the archived eyes with age-related macular degeneration. *Trans. Am. Ophthalmol. Soc.* **105**, 92–97, discussion 97–98 (2007).
30. A. Kanda *et al.*, Age-related macular degeneration-associated variants at chromosome 10q26 do not significantly alter ARMS2 and HTRA1 transcript levels in the human retina. *Mol. Vis.* **16**, 1317–1323 (2010).
31. U. Friedrich *et al.*, Risk- and non-risk-associated variants at the 10q26 AMD locus influence ARMS2 mRNA expression but exclude pathogenic effects due to protein deficiency. *Hum. Mol. Genet.* **20**, 1387–1399 (2011).
32. S. M. P. Jacobo, M. M. Deangelis, I. K. Kim, A. Kazlauskas, Age-related macular degeneration-associated silent polymorphisms in HtrA1 impair its ability to antagonize insulin-like growth factor 1. *Mol. Cell. Biol.* **33**, 1976–1990 (2013).
33. W. Samuel *et al.*, Appropriately differentiated ARPE-19 cells regain phenotype and gene expression profiles similar to those of native RPE cells. *Mol. Vis.* **23**, 60–89 (2017).
34. S. Peng *et al.*, Engineering a blood-retinal barrier with human embryonic stem cell-derived retinal pigment epithelium: Transcriptome and functional analysis. *Stem Cells Transl. Med.* **2**, 534–544 (2013).
35. I. Klimanskaya *et al.*, Derivation and comparative assessment of retinal pigment epithelium from human embryonic stem cells using transcriptomics. *Cloning Stem Cells* **6**, 217–245 (2004).
36. P. Choudhary *et al.*, Directing differentiation of pluripotent stem cells toward retinal pigment epithelium lineage. *Stem Cells Transl. Med.* **6**, 490–501 (2017).
37. L. Truebestein *et al.*, Substrate-induced remodeling of the active site regulates human HTRA1 activity. *Nat. Struct. Mol. Biol.* **18**, 386–388 (2011).
38. A. Tennstaedt *et al.*, Human high temperature requirement serine protease A1 (HTRA1) degrades tau protein aggregates. *J. Biol. Chem.* **287**, 20931–20941 (2012).
39. P. H. Chen *et al.*, High-temperature requirement A1 protease as a rate-limiting factor in the development of osteoarthritis. *Am. J. Pathol.* **189**, 1423–1434 (2019).
40. J. W. Crabb *et al.*, Drusen proteome analysis: An approach to the etiology of age-related macular degeneration. *Proc. Natl. Acad. Sci. U.S.A.* **99**, 14682–14687 (2002).
41. D. H. Anderson *et al.*, Characterization of beta amyloid assemblies in drusen: The deposits associated with aging and age-related macular degeneration. *Exp. Eye Res.* **78**, 243–256 (2004).
42. C. Knupp, S. Z. Amin, P. M. G. Munro, P. J. Luthert, J. M. Squire, Collagen VI assemblies in age-related macular degeneration. *J. Struct. Biol.* **139**, 181–189 (2002).
43. C. A. Curcio, M. Johnson, "Structure, function, and pathology of Bruch's membrane" in *Retina*, S. J. Ryan, Ed. (Elsevier, 2013), pp. 465–481.
44. M. Uemura *et al.*, HTRA1-related cerebral small vessel disease: A review of the literature. *Front. Neurol.* **11**, 545 (2020).
45. A. Joutel *et al.*, Notch3 mutations in CADASIL, a hereditary adult-onset condition causing stroke and dementia. *Nature* **383**, 707–710 (1996).
46. J. M. Schröder, B. Sellhaus, J. Jörg, Identification of the characteristic vascular changes in a sural nerve biopsy of a case with cerebral autosomal dominant arteriopathy with subcortical infarcts and leukoencephalopathy (CADASIL). *Acta Neuropathol.* **89**, 116–121 (1995).
47. M. E. Owen, T. P. Enevoldson, H. Heimann, Vitreous haemorrhage and ischemic retinopathy in a patient with CADASIL. *Graefes Arch. Clin. Exp. Ophthalmol.* **251**, 367–369 (2013).
48. F. Alten *et al.*, Multimodal retinal vessel analysis in CADASIL patients. *PLoS One* **9**, e112311 (2014).